Early Visuomotor Representations Revealed From Evoked Local Field Potentials in Motor and Premotor Cortical Areas

John G. O'Leary and Nicholas G. Hatsopoulos

J Neurophysiol 96:1492-1506, 2006. First published May 31, 2006; doi:10.1152/jn.00106.2006

J Neurophysiol 96: 1492–1506, 2006.
First published May 31, 2006; doi:10.1152/jn.00106.2006.

Early Visuomotor Representations Revealed From Evoked Local Field Potentials in Motor and Premotor Cortical Areas

John G. O'Leary and Nicholas G. Hatsopoulos
Department of Organismal Biology and Anatomy, University of Chicago, Chicago, Illinois

Submitted 31 January 2006; accepted in final form 25 May 2006

O'Leary, John G. and Nicholas G. Hatsopoulos. Early visuomotor representations revealed from evoked local field potentials in motor and premotor cortical areas. *J Neurophysiol* 96: 1492–1506, 2006. First published May 31, 2006; doi:10.1152/jn.00106.2006. Local field potentials (LFPs) recorded from primary motor cortex (MI) have been shown to be tuned to the direction of visually guided reaching movements, but MI LFPs have not been shown to be tuned to the direction of an upcoming movement during the delay period that precedes movement in an instructed-delay reaching task. Also, LFPs in dorsal premotor cortex (PMd) have not been investigated in this context. We therefore recorded LFPs from MI and PMd of monkeys (*Macaca mulatta*) and investigated whether these LFPs were tuned to the direction of the upcoming movement during the delay period. In three frequency bands we identified LFP activity that was phase-locked to the onset of the instruction stimulus that specified the direction of the upcoming reach. The amplitude of this activity was often tuned to target direction with tuning widths that varied across different electrodes and frequency bands. Single-trial decoding of LFPs demonstrated that prediction of target direction from this activity was possible well before the actual movement is initiated. Decoding performance was significantly better in the slowest-frequency band compared with that in the other two higher-frequency bands. Although these results demonstrate that task-related information is available in the local field potentials, correlations among these signals recorded from a densely packed array of electrodes suggests that adequate decoding performance for neural prosthesis applications may be limited as the number of simultaneous electrode recordings is increased.

INTRODUCTION

Although synchronous oscillations of neuronal populations have been observed throughout cortex, including in the visual, somatosensory, and motor cortices (Fetz et al. 2000; Fries et al. 2001; Lebedev and Nelson 1995), it is still unclear under what circumstances they may participate in the coding of sensory or motor information such as movement and target direction. Local field potentials (LFPs) recorded from penetrating microelectrodes represent the summed postsynaptic potentials of small populations of neurons and are thus considered to be an efficient measure of the synchronous and oscillatory activity of neurons in the cerebral cortex. In fact, LFPs may provide us with a view of such activity that cannot be obtained otherwise, given the difficulty of detecting synchrony and oscillations from multiple single-unit recordings.

Early studies of LFP activity in primate primary motor cortex (MI) found that LFPs engaged in beta and gamma oscillations (10–45 Hz) and that these oscillations occurred most often during steady postural configurations (Baker et al. 1999) or during hold periods that precede visually guided reaches and least often during the execution of these movements (Donoghue et al. 1998; Murthy and Fetz 1992, 1996a; Sanes and Donoghue 1993). Human EEG recordings have also shown movement-related desynchronization in the beta-frequency range (Gilbertson et al. 2005; Pfurtscheller et al. 2003, 2006). The results of these studies suggested that beta and gamma oscillations in MI were related to the degree of attention, movement anticipation, or the maintenance of a static posture because no features of these oscillations appeared to vary systematically with the sensory or movement features of the upcoming reach. However, more recent studies have presented evidence that challenges this view. In particular, LFP activity in MI was previously shown to vary with the direction of a reaching movement as it is being carried out (Mehring et al. 2003; Rickert et al. 2005), and LFPs in posterior parietal cortex were shown to modulate with the direction of reaches and saccades before they are executed (Scherberger et al. 2005).

Studies of the relationship between LFP activity and movement remain incomplete in at least two respects. First, LFPs in MI have been shown to be modulated by movement direction of reaches only during their execution; MI LFPs recorded when a delay separates a directional instruction from movement execution have not been shown to vary with movement direction. Second, LFPs in dorsal premotor cortex (PMd), a region thought to be important for planning movements, have not been examined. Although directional tuning of single units with MI and PMd during movement preparation has been well documented (Crammond and Kalaska 2000; Georgopoulos et al. 1989; Weinrich and Wise 1982), it is not obvious whether local field potentials that represent the summed postsynaptic potentials of hundreds of neurons (with potentially different preferred directions depending on their cell body distances) near the electrode tips would also be directionally tuned. In this study, we show that LFPs recorded from both MI and PMd contain information about the target direction to be reached and, in particular, that such information is present early in the preparatory period that precedes a reach in an instructed delay center-out task.

We characterized the extent to which LFP fluctuations in three frequency bands were modulated by target direction: fast oscillations in the gamma range (25–45 Hz), intermediate oscillations in the beta range (10–25 Hz), and slow fluctuations of $<$10 Hz in both MI and PMd. Unlike many previous studies that have examined non-phase-locked oscillations, we focused

Address for reprint requests and other correspondence: N. G. Hatsopoulos, Dept. of Organismal Biology and Anatomy, University of Chicago, Chicago, IL 60637 (E-mail: nicho@uchicago.edu).

The costs of publication of this article were defrayed in part by the payment of page charges. The article must therefore be hereby marked "*advertisement*" in accordance with 18 U.S.C. Section 1734 solely to indicate this fact.

on fluctuations in these three frequency bands that were phase-locked to the onset of the instruction signal initiating the preparatory period. We have identified phase-locked activity in each of these bands that emerges well before the onset of movement and is modulated by the direction of a visual instruction signal.

METHODS

Behavioral tasks

Three macaque monkeys (*Macaca mulatta*) were operantly trained to perform an instructed-delay eight-direction center-out (CO) task by moving a cursor to targets by arm movements. The left arm was used by two animals (monkeys B and RS) and the right arm was used by the other animal (monkey R). The task involved projecting the cursor and targets onto a horizontal, reflective surface in front of the monkey above the monkey's hand. The monkey's arm rested on cushioned arm troughs secured to links of a two-joint robotic arm (KINARM system; Scott 1999) underneath the projection surface. The shoulder joint was abducted 90° such that shoulder and elbow flexion and extension movements were made in the horizontal plane.

The CO task involved movements from a center target to one of eight peripherally positioned targets (distance of 5–7 cm). On each trial, one of the eight peripherally positioned targets was pseudorandomly selected. The task consisted of three epochs: *1*) a 400- or 500-ms hold period during which the monkey was required to hold its hand over the center target; *2*) a fixed instruction period of 600 or 1,000 ms or a variable instruction period of 1,000 to 1,500 ms (depending on the recording session), during which one of the eight final targets appeared, although the monkey was not allowed to move; and *3*) a "go" period during which the target began to blink, informing the monkey to begin moving to the peripherally positioned target.

Electrophysiology

Two silicon-based electrode arrays (Cyberkinetics Neurotechnology Systems, Foxboro, MA) composed of 100 electrodes (electrode length 1.0 mm; interelectrode separation 400 μm) were implanted in the contralateral arm areas of primary motor (MI) and dorsal premotor (PMd) cortices of each monkey (Fig. 1) (see Hatsopoulos et al. 2004 for more information about the placement of the arrays in the two cortical areas and Maynard et al. 1999 for more details concerning the electrode array). Based on histological evidence from previous implants that we have performed, the electrode tips are likely to be in lower portions of layer 3 or in layer 5. During a recording session, LFP signals were amplified (gain, 5,000), band-pass filtered (0.3–250 or 0.3–500 Hz), and recorded digitally (14-bit) at 1 kHz per channel from ≤256 sites over both arrays simultaneously using one or two Cerebus acquisition systems (Cyberkinetics Neurotechnology Systems).

A total of nine data sets (four each from animals B and R and one from animal RS) were analyzed, where a data set is defined as all simultaneously recoded neural data collected in one recording session. We removed data from electrodes that either exhibited no signal amplitude (resulting from a broken connection or head-stage amplifier) or large amounts of 60-Hz line noise. After removing these channels, each data set contained between 87 and 164 simultaneously recorded sites from MI and PMd (Table 1). We then isolated the fast (25–45 Hz), intermediate (10–25 Hz), and slow (<10 Hz) signal types by digitally band-pass filtering or low-pass filtering the LFP signals using eighth-order Butterworth filters designed in Matlab (The MathWorks, Natick, MA). The filters were applied forward and backward in time to eliminate any phase distortion. The full-bandwidth (DC to about 250 or 500 Hz) LFP at time t for the cth channel and the ith trial will be referred to as $LFP^{b}_{c,i}(t)$, and the LFP in the slow, intermediate, and fast bands will be referred to as $LFP^{b}_{c,i}(t)$, respectively, where b is the name of the band to which we are referring. All subsequent analyses were performed using Matlab and its Signal Processing, Statistics, Optimization, and Wavelet Toolboxes.

TABLE 1. *Number of trials and channels recorded per data set*

	Total Number of Trials	MI Electrodes	PMd Electrodes	Total Number of Electrodes
b030314	409	48	39	87
b030416	717	51	40	91
b030710	546	41	57	98
b030722	447	39	57	96
r031215	372	89	29	118
r040123	217	60	63	123
r040130	277	32	93	125
r040222	463	59	60	119
rs050225	391	94	70	164
Total		513	508	1,021

To acquire extracellular action potentials, signals were band-pass filtered (250 Hz to 7.5 kHz) and sampled at 30 kHz per channel. Only waveforms that crossed a threshold were stored and spike-sorted using Offline Sorter (Plexon, Dallas, TX). Interspike interval histograms were computed to verify single-unit isolation by ensuring that <0.05% of waveforms possessed an interspike interval <1.6 ms. Signal-to-noise ratios were defined as the difference in mean peak-to-trough voltage divided by twice the SD. All isolated single units used in this study possessed signal-to-noise ratios of ≥4:1. Spike data were acquired from six (four data sets for animal B, one data set for animal R, and one data set from animal RS) of the nine data sets from which LFP data were recorded. Each data set contained between 34 and 141 simultaneously recorded units from both areas. A total of 272 and 192 single units were recorded from MI and PMd, respectively, over all six data sets. Both ensembles consisted of "randomly" selected units from MI and PMd except for a possible bias for neurons with large cell bodies that would generate higher signal-to-noise ratios. All of the surgical and behavioral procedures were approved by the University of Chicago's IACUC and conform to the principles outlined in the Guide for the Care and Use of Laboratory Animals (National Institutes of Health publication no. 86–23, revised 1985).

Directional tuning of LFPs

For each channel, we determined separately whether the fast, intermediate, or slow activity that followed the instruction signal was tuned to target direction and also whether these three bands of activity surrounding the onset of movement were directionally tuned. One method was used for the fast and intermediate bands and a slightly

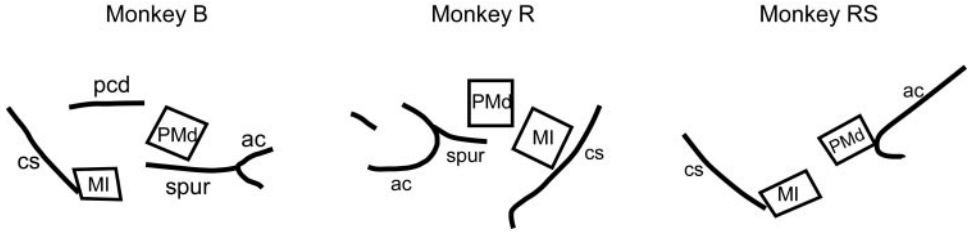

FIG. 1. Placement of the 2 electrode arrays in the primary motor (MI) and dorsal premotor (PMd) cortices of the 3 monkeys based on digital photographs taken during the surgical implantation. CS, central sulcus; ac, arcuate sulcus; psd, precentral dimple; spur, spur of the arcuate sulcus.

different method was used for the slow band. The general procedure for each combination of channel, band, and behavioral event was as follows: first, a feature of the signal, $\phi^{b}_{c,i}$, was computed for each trial i from the LFP of the band b and channel c of interest. These features were grouped based on the target direction associated with the trial from which they were derived and an ANOVA was performed to test whether the feature varied with target direction. For each channel for which the ANOVA indicated a directional effect, the mean of the feature for each target direction was then computed and a tuning curve was fit to those means. If the tuning curve fit the data well ($R^2 > 0.7$, $P < 0.01$), we then extracted the preferred direction of the channel from that curve.

The difference between the procedures followed for the fast and intermediate bands and those followed for the slow band came in the choice of feature derived from each trial. For the fast and intermediate bands, the root-mean-square (RMS) LFP between 50 and 200 ms after the onset of the instruction signal was used. That is, for channel c and trial i, $\phi^{fast}_{c,i}$, the RMS LFP for the fast band is given by

$$\phi^{fast}_{c,i} = \sqrt{\frac{1}{151}\sum_{t=50}^{200}[LFP^{fast}_{c,i}(t)]^2}$$

For the slow band, a baseline slow LFP was first determined for the trial by averaging the LFP during the hold period before the onset of the instruction signal. This baseline LFP, $\overline{LFP}^{slow}_{c,i}$, was subtracted from the voltage record for the whole trial, the potentials were inverted (to aid in the comparison of tuning curves across bands), and this inverted, baseline-corrected LFP was integrated from 50 to 350 ms after instruction onset

$$\phi^{slow}_{c,i} = \sum_{t=50}^{350} -[LFP^{slow}_{c,i}(t) - \overline{LFP}^{slow}_{c,i}]$$

We used essentially the same formulas to derive the signal features we used to the determine the perimovement preferred directions of the LFPs, the only difference being that the summation ran from −200 to 200 ms with respect to movement onset. We determined the preferred directions based on these features of the signal because visual inspection of the band-limited LFPs averaged by direction and triggered on the instruction or the start of movement suggested they would allow us to represent reasonably well with a single number those aspects of the signal that varied with direction.

In all cases, we used a tuning function based on the probability density function of the von Mises distribution, which is the circular statistics analogue of the normal distribution (Amirikian et al. 2000; Fisher 1993), which we call a *VM function*, defined as a scaled and shifted version of the VM pdf

$$\phi^{b}_{c}(\theta; m, s, \mu, \kappa) = m + \frac{s}{2\pi I_0(\kappa)} e^{k\cos(\theta-\mu)} \quad 0 \le \mu < 2\pi, 0 \le \kappa < \infty$$

In this function, θ is the direction for which the feature is being estimated and m, s, μ, and κ are tunable free parameters. The parameter m represents the minimum value of the feature, s gives the scale of its stimulus-induced modulation, μ represents the preferred direction, and κ changes the sharpness of the tuning. We included the normalization factor of the von Mises pdf, $2\pi I_0(\kappa)$ (where I_0 is the modified Bessel function of the first kind and order zero), because it was found to aid curve fitting. We elected to use the VM function because the LFPs were often too sharply tuned to be well fit by the more common cosine tuning function. We fit the data to the VM function with a stringent threshold value for R^2 of 0.7 ($P < 0.01$, t-test) compared with the more standard threshold of 0.5 used for cosine tuning of single units because of the extra tuning width parameter that was absent in the cosine function.

Directional tuning of single units

A standard cosine function was fit to the average firing rate of each single unit over all eight target directions (Georgopoulos et al. 1982). The instruction-related tuning curve was based on the trial-averaged spike counts measured from 50 to 350 ms relative to the instruction signal onset. The movement-related tuning curve was based on the trial-averaged spike counts measured from −200 to +200 ms with respect to movement onset.

Frequency domain analyses

We determined the overall frequency content of the early instruction period LFPs recorded by each channel by computing discrete Fourier transforms (DFTs) of the unfiltered LFP, $LFP_{c,i}(t)$, recorded during the first 500 ms after the onset of the instruction, squaring the modulus of the DFT coefficients to obtain power and then averaging power across trials. Data were tapered with a Hanning window before performing a 500-point DFT to yield a frequency resolution of 2 Hz.

To test whether activity in each frequency band was phase-locked to the instruction signal, DFTs were performed on Hanning-tapered 256-ms sections of each signal to yield a frequency resolution of 3.9 Hz. A phase angle was then determined for each frequency on each trial by computing the four-quadrant arctangents of the associated DFT coefficients, after which the degree of phase-locking (that is, the trial-by-trial consistency of phase angles) at each frequency was then quantified by performing a Rayleigh test on the sample of angles associated with that frequency. We then examined the results of the Rayleigh tests for each frequency at which the DFT was computed and classified a band recorded from a channel as phase-locked if at least one of the frequencies within that band was phase-locked. For example, because the DFT was evaluated at 3.9 and 7.9 Hz, and these frequencies were within the low-frequency band (but the next frequency, 11.7 Hz, was not), a channel was classified as phase-locked in the low-frequency band if its activity at either or both of these frequencies was phase-locked. We thus rejected one null hypothesis (no phase-locking within a band) based on the results of multiple statistical tests. If a null hypothesis is rejected or accepted based on the results of multiple statistical tests, one can use the inclusion–exclusion principle to determine the fraction of null hypotheses one expects to reject by chance. Assuming the tests are independent, this fraction, f_{Chance}, is given by

$$f_{Chance} = \binom{n}{1}\alpha - \binom{n}{2}\alpha^2 + \cdots + (-1)^{n-1}\binom{n}{n}\alpha^n$$

where n is the number of statistical tests that will be carried out to test each null hypothesis and α is the significance level of each test.

To gain some sense of how the degree of phase-locking changes on a fine timescale during a trial, and how the degree of phase locking varies across target direction, a time–frequency phase-locking analysis was performed separately on the trials from each direction. This analysis was performed in essentially the same fashion as the phase-locking analysis described above, except that the continuous wavelet transform was substituted for the DFT and the trials were pooled by direction. In the continuous wavelet transform, wavelet coefficients are determined at a series of points in the time–frequency plane by convolving a mother wavelet, centered in time and frequency at that point, with the signal to be analyzed. We chose as our mother wavelet the Complex Morlet wavelet, which is defined in the Matlab Wavelet Toolbox by bandwidth and center frequency parameters, both of which we set to 1. When this wavelet is convolved with the signal at a time–frequency point, a complex-valued coefficient results, and the phase angle of the signal at that time–frequency point can be determined by taking the four-quadrant arctangent of that coefficient (Tallon-Baudry et al. 1996). We did this for each trial and then used a Rayleigh test to determine whether the resulting sample of phase angles for each direction was likely to have been drawn from a

uniform distribution. We used a time axis that ran from the beginning of the hold period to the end of the instruction period and a frequency axis that ran from 1 to 40 Hz in 0.5-Hz increments.

Single-trial decoding of direction

To decode target direction from single-trial LFPs, it was again necessary to represent each trial with a vector of features. To this end, in each of our three bands we averaged $LFP^b_{c,i}$ across time bins of sufficiently small size that the Nyquist frequency of the decimated time series would be greater than or equal to the maximum frequency in that band. We chose as time intervals over which to bin the data the most similar time intervals possible to those used for the derivation of the preferred-direction features because the bin sizes we used did not evenly divide the preferred-direction time intervals. Thus each $LFP^b_{c,i}$ was represented by a series of bins, each representing the average LFP in that channel, band, and trial during a portion of the instruction period. Vectors for classification were then created for each trial by concatenating these decimated time series from multiple channels. The specific bin sizes and time ranges used were: 50-ms bins from 51 to 350 ms relative to the onset of the instruction signal for the slow band, 20-ms bins from 46 to 205 ms for the intermediate band, and 10-ms bins from 51 to 200 ms for the fast band.

Fisher's linear discriminant analysis (Klecka 1980) was used to predict target direction from each vector of binned instruction period activity. Classification performances given were obtained using leave-one-out cross-validation, in which a classification rule is estimated from the data for all trials but one and then the "left-out" trial is classified using the rule. This is repeated until all trials in the data set have been left out, after which generalization performance is estimated as the percentage of left-out trials that were correctly classified.

RESULTS

Fast, intermediate, and slow fluctuations

We investigated three forms of LFP activity in motor cortex that are present during the ostensible planning of a visuomotor reaching behavior. As in MI, the LFP signal in PMd (Fig. 2*A*) is composed of fast (gamma band) and intermediate oscillatory (beta band) activity, which can be isolated by band-pass filtering the signal between 25 and 45 Hz (Fig. 2*B*) and between 10 and 25 Hz (Fig. 2*C*), respectively. The slow fluctuating activity is isolated by low-pass filtering the signal <10 Hz (Fig. 2*D*). As has been demonstrated in MI, the beta oscillations in PMd decrease in amplitude after the onset of the go cue and remain at a minimum throughout the movement period. The slow fluctuation is evident as a negative deflection after the instruction signal. We chose the three frequency bands used in the preceding decomposition by examining the grand average power spectrum for each channel, computed from the first 500 ms of the instruction period as described in METHODS.

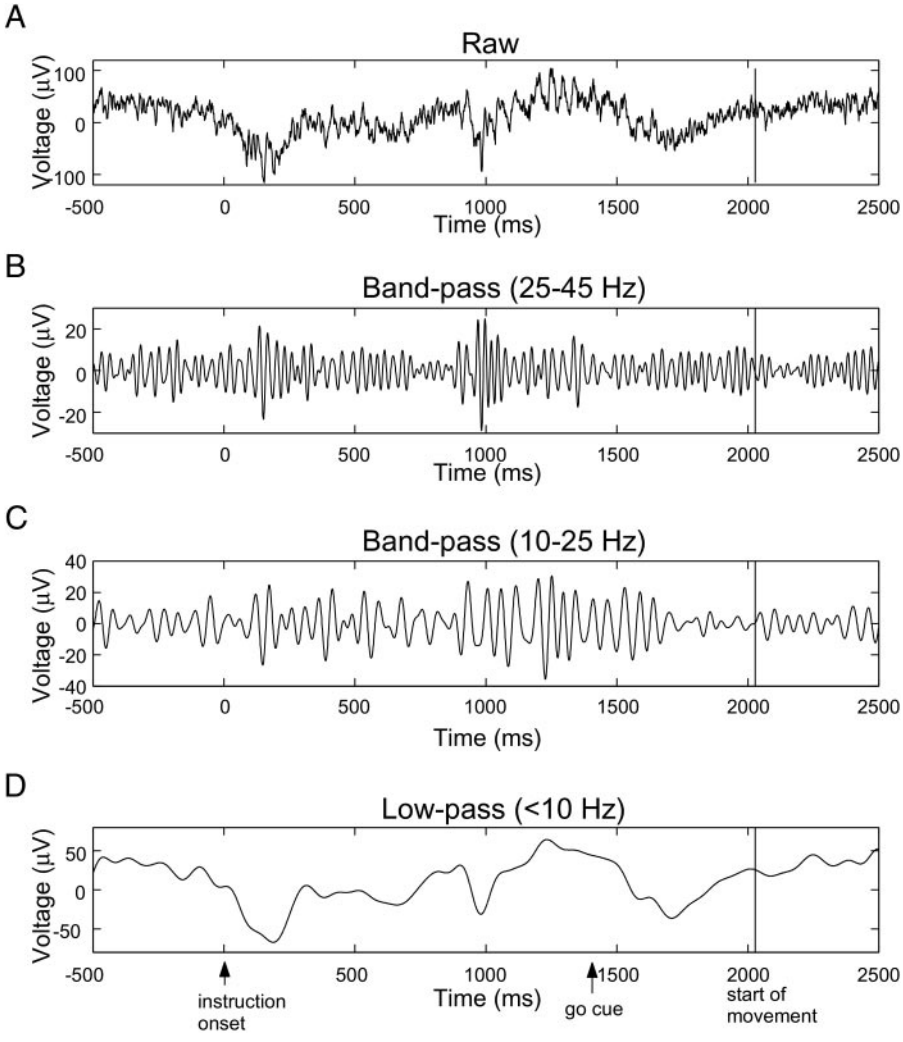

FIG. 2. Local field potential (LFP) signal recorded from one electrode implanted in the PMd cortex during one trial of the center-out task. *A*: raw acquired LFP signal filtered between 0.1 and 250 Hz during acquisition. *B*: band-pass (25–45 Hz) filtered LFP signal revealing fast (gamma) oscillations. *C*: band-pass (10–25 Hz) filtered LFP signal revealing intermediate (beta) oscillations, particularly evident during the instruction period. *D*: low-pass (<10 Hz) filtered LFP signal revealing slow fluctuations. Notice the negative deflection after the instruction signal.

The power spectra in both cortical areas most often exhibited peaks in the beta range and frequently were marked by peaks in the gamma range as well (Fig. 3, *A–C*). Although only power spectra from MI of animal RS were marked by local maxima in the slow range (Fig. 3*C*), all channels from all animals displayed a large amount of power in this range, and thus we decided to examine slow activity in all animals. Distributions of local power spectral peaks over all data sets are shown in Fig. 3*D*. Time–frequency spectrograms during the instruction period confirm dominant power in all three frequency bands (Fig. 4). These spectrograms also suggest that there is directional modulation in power in multiple frequency bands at different epochs of the instruction period (see *Direction tuning* below).

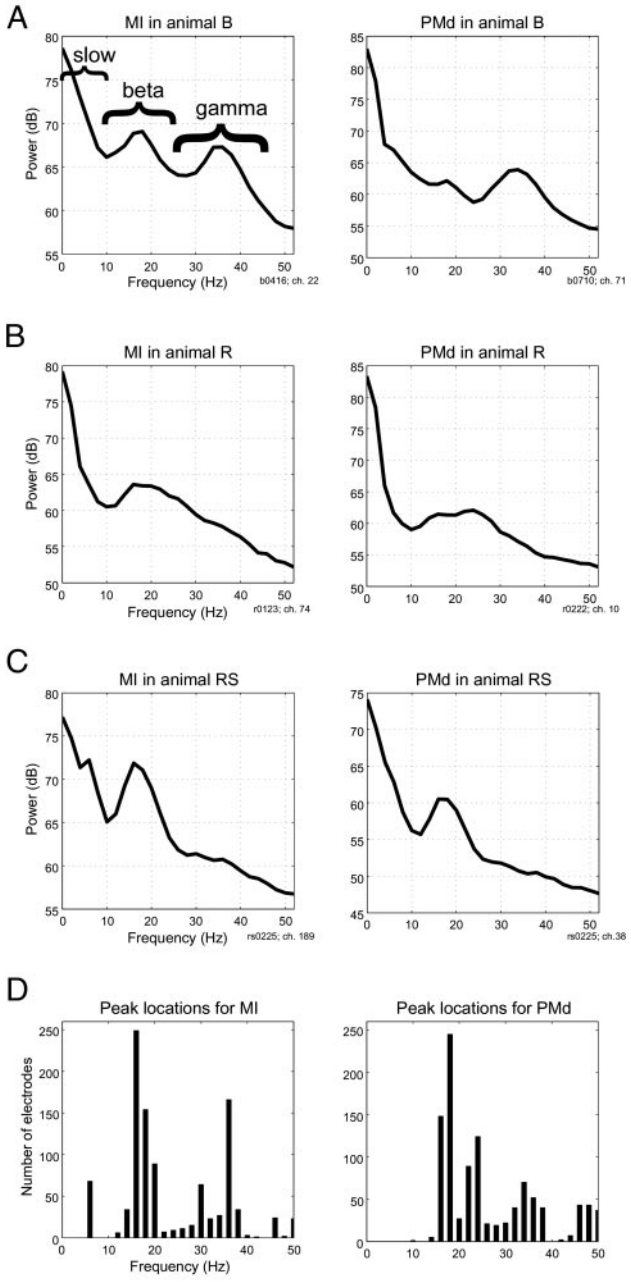

FIG. 3. Power spectra averaged over multiple trials of LFP signals from MI and PMd revealing local peaks in the beta and gamma ranges as well as strong signal power in the low-frequency range (<10 Hz). *A*: power spectra of LFP signals from MI (*left*) and PMd (*right*) in one monkey. Two peaks in the beta and gamma ranges were evident in this monkey. *B* and *C*: same as *A* for the second and third monkeys. *D*: histogram tabulating the frequency of occurrence of local peaks in power <45 Hz over all electrodes in MI (*left*) and PMd (*right*) in all 3 monkeys.

Phase-locked activity

We observed LFP activity phase-locked to the onset of the instruction signal for fast (gamma band), intermediate (beta band), and slow fluctuations. We isolated this activity on each channel by averaging the band-limited LFPs across all trials, triggered on the onset of the instruction signal (Fig. 5). We refer to this instruction-triggered average potential as the *instruction-evoked potential*, or IEP.

IEPs in the intermediate and fast bands were observed on most channels and were present only at the beginning of the instruction period. Because it has been well documented that non-phase-locked activity is present in these bands after an instruction signal (Murthy and Fetz 1992; Sanes and Donoghue 1993), we sought to verify that IEPs we observed based on the averaged potentials were the product of activity that was phase-locked to the instruction onset. We thus measured the trial-by-trial consistency of the signal's phase in different parts of the time–frequency plane (see METHODS; Shah et al. 2004). A highly significant departure from uniformity indicated a highly consistent phase relationship across trials (Fig. 6). Phase-locked activity was observed more often in the intermediate band than in the fast band and was almost entirely restricted to the period immediately after the onset of the instruction signal. In the intermediate band, 902 of the 1,021 (88%; 85% in MI and 91% in PMd) channels contained statistically significant phase-locking on at least one of the frequencies in that band during the first 256 ms of the instruction period ($P < 0.01$, Rayleigh test), whereas in the fast band, 557 (55%; 53% in MI and 56% in PMd) of the channels met this criterion. Meanwhile, only 134 (13%) and 53 (5%) of the channels contained significant phase-locked activity in the intermediate and fast bands, respectively, during the second 256 ms after the instruction signal onset. We also examined the degree of phase-locking during the 256 ms before the instruction stimulus was presented and found that 56 (5%) and 11 (1%) of the channels had significant phase-locked activity in the intermediate and fast bands, respectively, during that period ($P < 0.01$, Rayleigh test). These results demonstrated that the intermediate- and fast-frequency phase-locking occurred transiently as a consequence of the onset of the instruction stimulus and was not a phenomenon that reflected stimulus anticipation.

The slow IEP appeared on all channels and consisted of one or more negative deflections followed sometimes by a positive deflection. Phase-locking was even more prevalent in the slow-frequency band: 1,005 of the 1,021 channels (98%; 98% in MI and 99% in PMd) contained significant phase-locking in the slow-frequency band during the first 256 ms after the instruction signal onset ($P < 0.01$, Raleigh test). In contrast to the intermediate- and fast-frequency bands, there was also considerable phase-locking in the second 256 ms after the instruction signal onset where 893 of the 1,021 channels (87%) exhibited significant phase-locking. This suggests that phase-locking is a much more sustained phenomenon in the slow-frequency band.

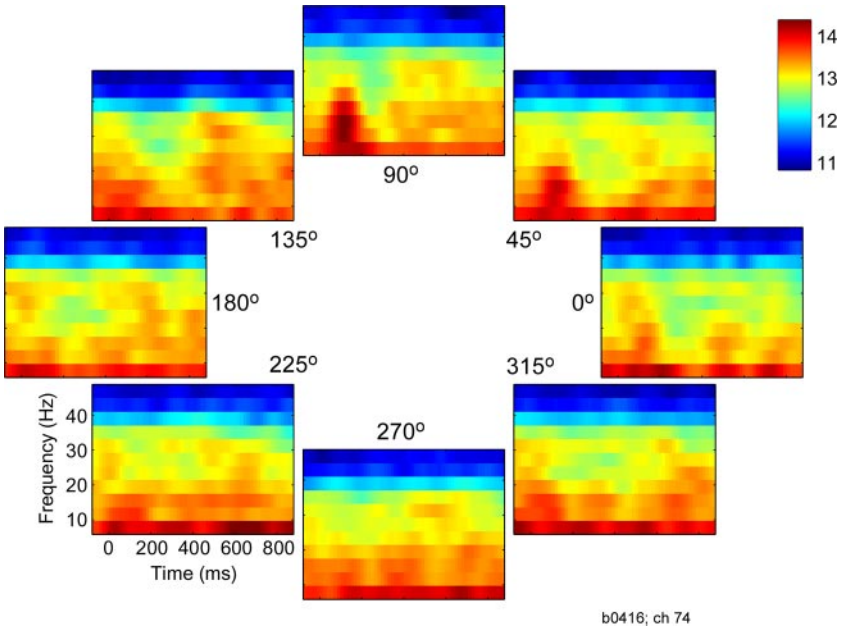

FIG. 4. Time–frequency spectrograms of raw LFP from one channel recorded in PMd over all 8 target directions. For each target direction, single-trial spectrograms were computed and then averaged.

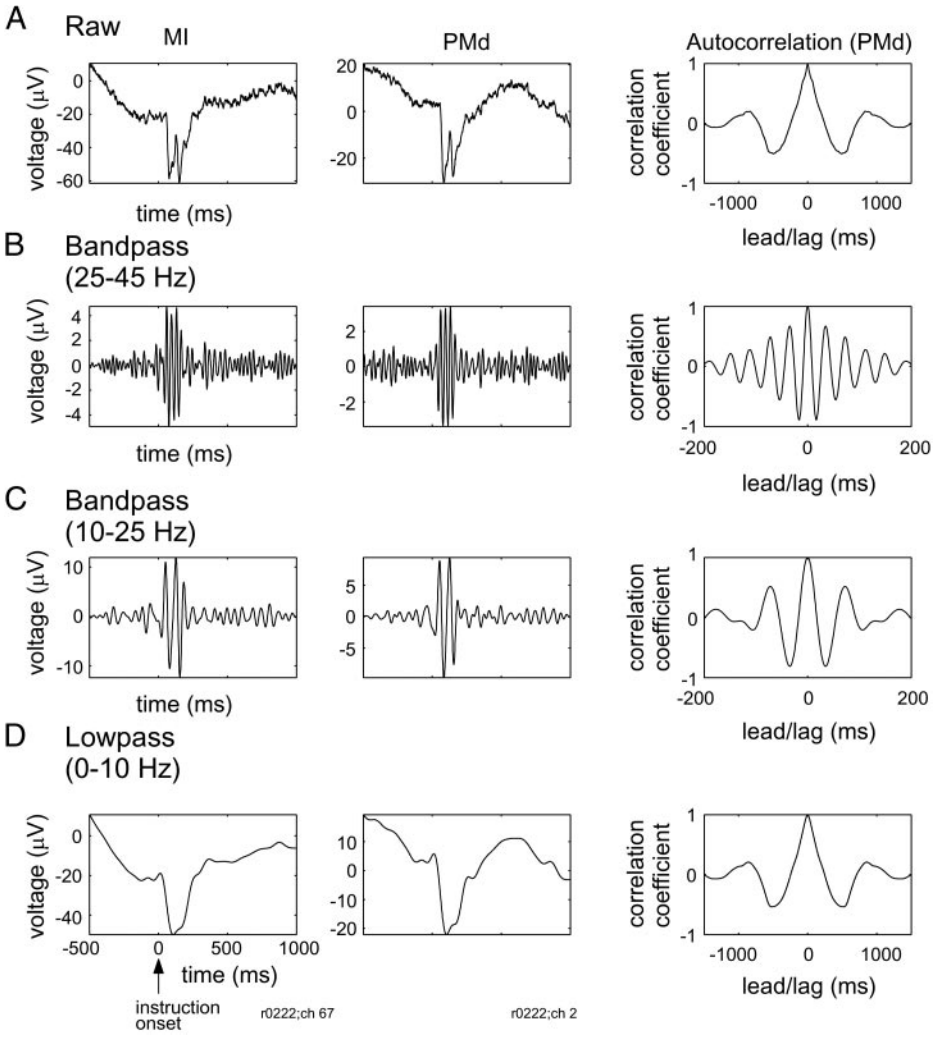

FIG. 5. Instruction-evoked potential (IEP) recorded from 2 electrodes implanted in the primary motor cortex (MI; *left*) and dorsal premotor (PMd; *middle*) cortex averaged over all trials, and the autocorrelation function of the IEP from PMd (*right*). *A*: raw IEPs filtered between 0.1 and 250 Hz during acquisition. *B*: IEPs based on the average of band-pass (25–45 Hz) filtered LFP signals revealing phase-locked fast oscillations. *C*: IEPs based on the average of band-pass (10–25 Hz) filtered LFP signals revealing phase-locked intermediate (beta) oscillations. *D*: IEPs based on the average of low-pass (<10 Hz) filtered LFP signals revealing phase-locked slow fluctuations.

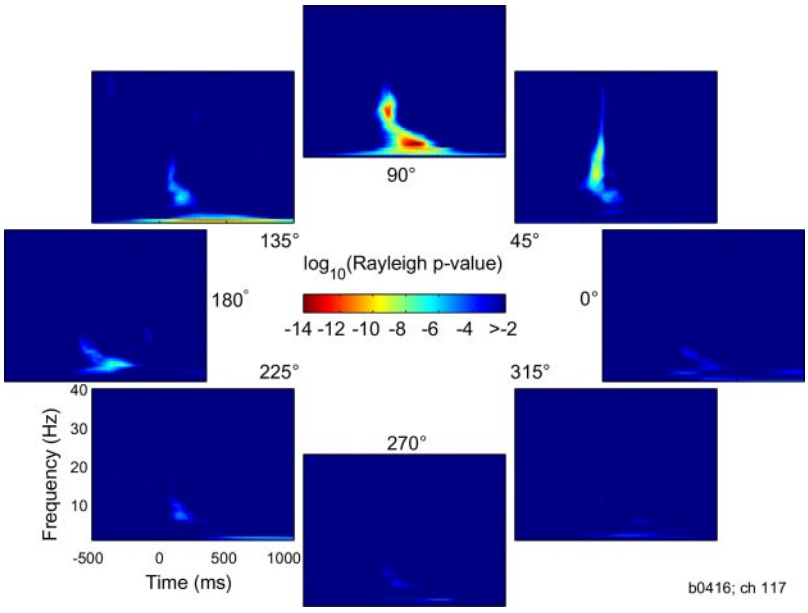

FIG. 6. Phase-locking of the LFP oscillation recorded in PMd with respect to the onset of the instruction signal for each of the 8 directions. Each panel plots the degree of phase-locking (color) as a function of frequency and time during the trial. Degree of phase-locking is denoted by the *P* value of Rayleigh test for uniform phase angles over all trials in a particular direction. Highly significant phase-locking is evident for all 3 frequency bands. Each of the panels is positioned in accordance with the direction of the target to be reached.

Latency of the IEP

Because the intermediate and fast IEPs typically lasted multiple cycles, and the number and phase of the cycles often varied across channels, it was problematic to use the timing of a single peak to characterize their latencies. We therefore computed the root-mean-square (RMS) IEP in a 151-ms window whose left edge we advanced from 1 to 106 ms in 1-ms steps. When the RMS IEP was at its peak, we designated the time at the center of the window the latency of the intermediate or fast IEP. Using this measure, the intermediate IEP peaked first in PMd, at 114 ± 25 ms (mean ± SD) after the onset of the instruction signal and, later in MI, at 122 ± 23 ms. Meanwhile, the fast IEP peaked first in MI, at 105 ± 24 ms, and later in PMd, at 118 ± 22 ms. Both of these differences in timing were significant ($\chi^2 = 61.96$ for intermediate, $\chi^2 = 57.36$ for fast; $P < 0.001$, Kruskal–Wallis tests).

We characterized the slow IEP latency in terms of the timing of the first negative peak to appear after the onset of the instruction signal. The timing of this peak was determined by having an automated algorithm find the first time after the instruction signal at which the first derivative of the IEP crossed zero and the second derivative of the IEP was negative. Visual inspection confirmed that this algorithm generally identified a reasonable latency. This peak arrived first in MI, at 113 ± 30 ms, and second in PMd, at 123 ± 33 ms ($\chi^2 = 55.97$; $P < 0.001$, Kruskal–Wallis test). In animal RS, a second negative deflection regularly appeared at consistent latencies across all channels and, in animal B, a similar deflection appeared across channels and data sets in PMd. This peaked at 261 ± 50 ms in MI and at 269 ± 37 ms in PMd.

Direction tuning

As has been well documented for single units within motor cortex (Georgopoulos et al. 1982) as well as for field potentials evoked with respect to movement (Rickert et al. 2005), directional tuning in the magnitude of the IEP (the LFP mean voltage averaged over multiple trials from the same direction condition) was observed in all three bands (Fig. 7), as suggested by the time–frequency spectrograms in Fig. 4. As described more fully in METHODS, to identify directionally tuned activity we first reduced the LFP in each band to a single value and tested for an effect of direction on that feature of the signal. This was accomplished by performing a one-way ANOVA on each channel and frequency band separately and testing for a main effect of direction. Of the 1,021 channels, 483 (47%; 44% in MI and 51% in PMd), 162 (16%; 14% in MI and 18% in PMd), and 518 (51%; 50% in MI and 51% in PMd) had a directional effect in the fast, intermediate, and slow bands, respectively ($P < 0.05$, ANOVA). We then tested whether the feature varied smoothly with direction by fitting a VM function to the values of the derived features. Of those channels showing a directional effect, VM functions fit ($R^2 > 0.7$, $P < 0.01$) the fast features of 120 channels (22 and 28% of all MI and PMd channels, respectively, that showed a directional effect based on the ANOVA test), the intermediate features of 60 channels (19 and 51% of all MI and PMd channels, respectively), and the slow features of 277 channels (63 and 44% of all MI and PMd channels, respectively).

A few trends became apparent when these preferred directions with respect to the instruction signal were examined across cortical areas and data sets (Fig. 8, *A–C*). First, within a cortical area and frequency band in a given data set, the PDs were not uniformly distributed around the circle but instead tended to cluster in relatively few—and often just one—compact modal groups. These clusters were generally consistent across both cortical areas for those few data sets that exhibited directional tuning in both cortical areas (Fig. 8, *A–C*, scatterplots) except in the slow-frequency range. For slow IEPs in MI, PD clusters tended to occur within three of the four quadrants with only seven channels representing directions between 90 and 180° (Fig. 8*C*, *left polar plot*), whereas in PMd, the clusters tended to occur between 90 and 270° (Fig. 8*C*, *right polar plot*). In a comparison of PDs across different frequency bands, we found no significant correlation in directional tuning between any pair of bands within MI or PMd. In contrast to the local field potential PDs, we did not observe

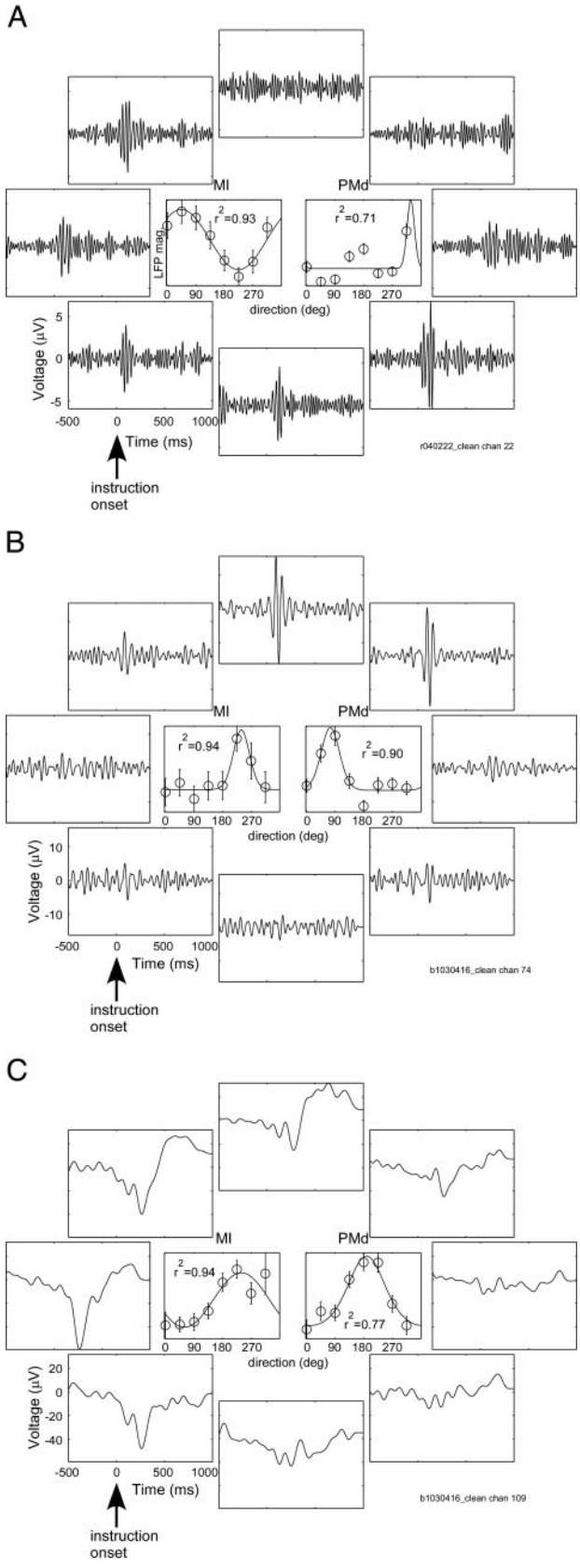

clustering among instruction-related single-unit PDs within either MI or PMd (Fig. 8*D*).

We also compared the directional tuning of IEPs with the tuning of local field potentials evoked with respect to onset of the arm movement (Fig. 8, *E–G*). Movement-evoked potentials (MEPs) in MI and their modulation with movement direction were documented by previous research (Mehring et al. 2003; Rickert et al. 2005). We observed directional tuning in the MEPs in all three frequency bands and their preferred directions were generally consistent across both cortical areas (Fig. 8, *E–G*, scatterplots). As with the IEPs, distributions of PDs among MEPs in all three frequency bands were highly clustered, which was not evident among the movement-related single-unit PDs (Fig. 8*H*).

The preferred directions of individual-channel IEPs and MEPs were significantly correlated in the fast-frequency band within both MI ($r+ = 0.63$, $P < 0.01$) and PMd ($r+ = 1$, $P < 0.01$) as well as in the slow-frequency band within both MI ($r+ = 0.63$, $P < 0.05$) and PMd ($r+ = 1$, $P < 0.01$). It should be noted that $r+$ represents the circular correlation coefficient (necessary for circular variables such as direction) and not a standard correlation coefficient (Batschelet 1981). The distribution of PD differences between IEPs and MEPs was centered at zero for the fast-frequency band for both MI (Fig. 9*A*, black bars) and PMd (Fig. 9*A*, white bars). The reason for the few number of samples in the fast-frequency band (Fig. 9*A*) is explained by the paucity of channels that simultaneously exhibited both IEP and MEP directional tuning. The majority of PD differences in the slow-frequency band were offset from zero within both MI (Fig. 9*C*, black bars) and PMd (Fig. 9*C*, white bars), which indicates that the IEP and MEP preferred directions are different despite their correlation. The IEPs and MEPs were not significantly correlated in the intermediate-frequency band (Fig. 9*B*). Interestingly, the instruction-related and movement-related PDs among single units were highly correlated and similar within MI (Fig. 9*D*, black bars) but not in PMd (Fig. 9*D*, white bars).

The widths of the VM directional tuning curves for both IEPs and MEPs exhibited a diversity of values, although they tended to cluster in certain ranges. For IEPs (Fig. 10, *A–C*), tuning curves were either broadly tuned (about 90°) or sharply tuned (10–40°) for the fast- and slow-frequency bands. In the fast (gamma) band, MI exhibited predominantly broad tuning, whereas PMd exhibited sharp tuning (Fig. 10*A*). In the slow band, in contrast, PMd channels were mostly broadly tuned, whereas MI were both broadly and sharply tuned (Fig. 10*C*). In the intermediate (beta) band, tuning curve widths ranged predominantly from 10 to 40° for both MI and PMd (Fig. 10*B*). For MEPs (Fig. 10, *D–F*), tuning was predominantly broad (about 70–90°) for all frequency bands and cortical areas. The very sharp tuning (e.g., <30°) that was occasionally observed should be considered with some caution given the limited resolution of these experiments using only eight target directions.

FIG. 7. Directional tuning of IEPs. *A*: IEPs (averaged potentials over multiple trials per direction condition) in the fast-frequency range over all directions for a channel recorded in PMd. Layout of panels is in accordance with direction of target to be reached. Two panels in the *center* plot the LFP mean (over multiple trials) magnitude vs. direction along with the best-fit von Mises function for a channel in MI and one in PMd. Error bars represent SEs. *B* and *C*: same as *A*, except for intermediate and slow IEPs, respectively.

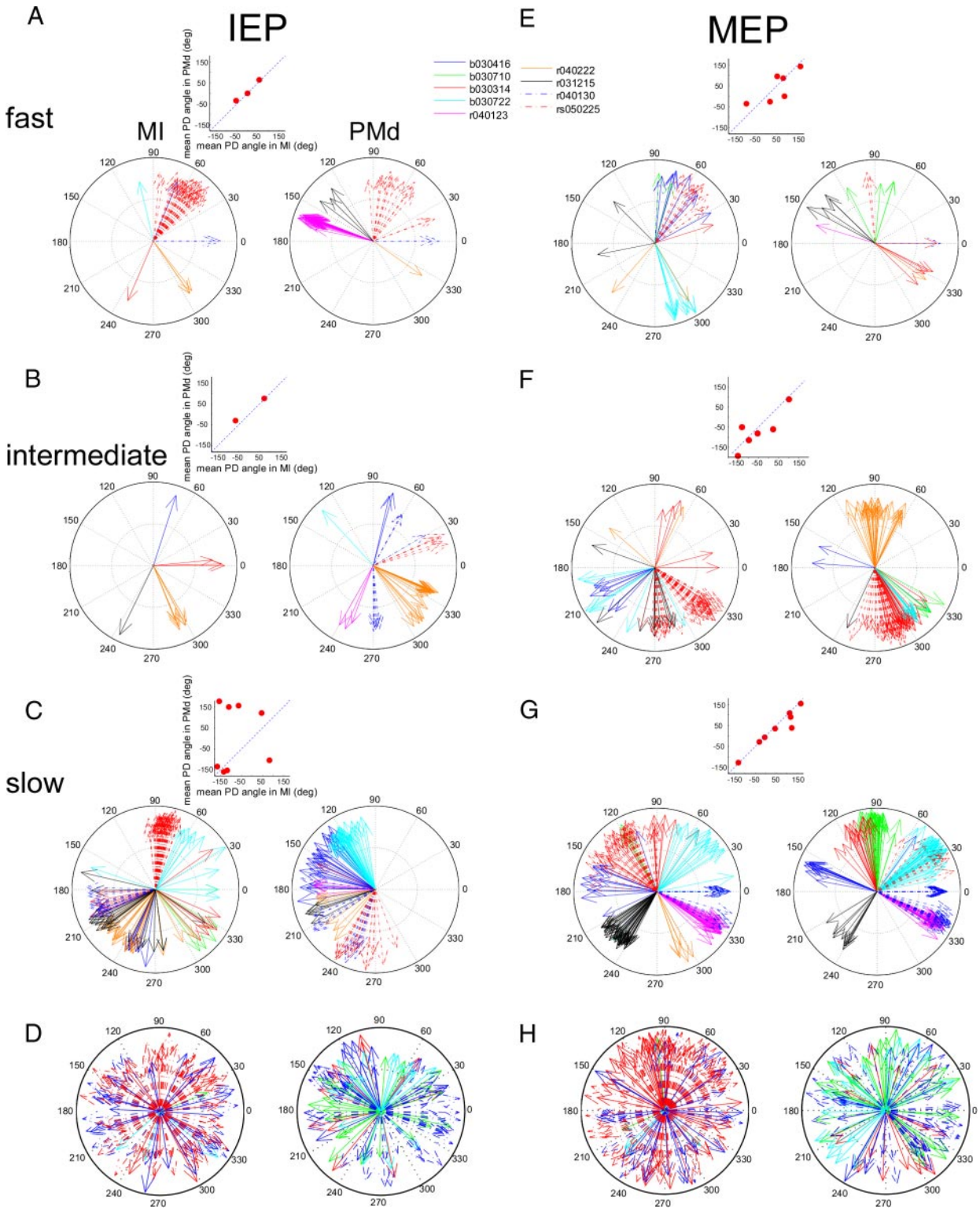

FIG. 8. Preferred directions of IEPs and movement evoked potentials (MEPs) for all 3 frequency bands in both cortical areas. Magnitudes of the preferred-direction vectors correspond to the R^2 values of the fits to the von Mises tuning function. Only R^2 values > 0.7 are plotted ($P < 0.01$). *A–C*: plots of preferred-direction vectors for IEPs. *D*: plot of instruction-related preferred-direction vectors among single units from 6 of the 9 data sets based on a cosine tuning function. Only R^2 values > 0.5 are plotted ($P < 0.05$). *E–G*: plots of preferred-direction vectors for MEPs. *H*: plot of movement-related preferred-direction vectors among single units from 6 of the 9 data sets. Scatterplots above of each pair of compass plots compare the circular mean preferred directions (mean over channels within a data set) within MI vs. PMd across all data sets in which directional tuning was observed in both MI and PMd. Points falling close to the identity line (dashed line) indicate that the preferred directions were similar across the 2 cortical areas.

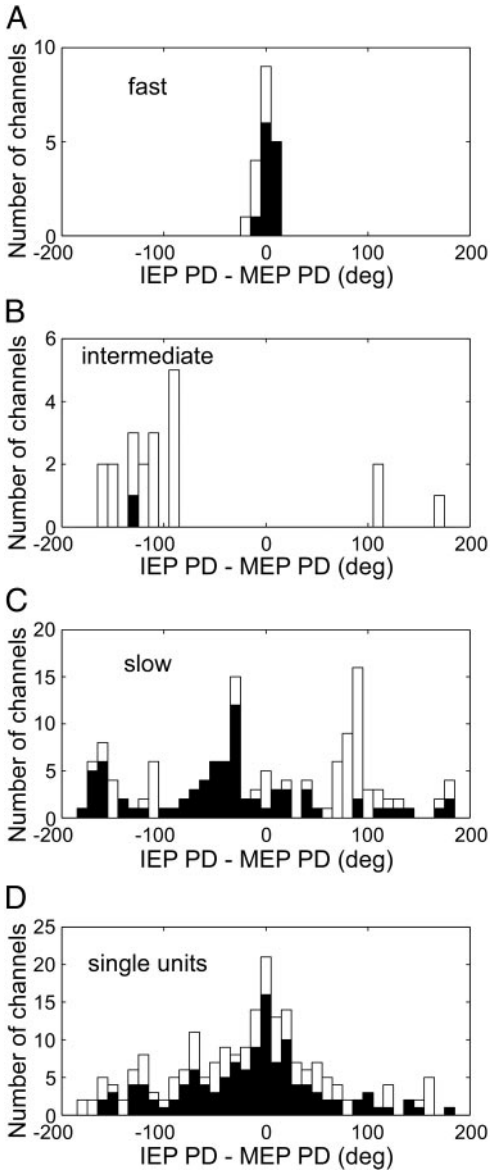

FIG. 9. Distribution of differences between IEP and MEP preferred directions within MI (black bars) and PMd (white bars). Difference histograms between IEP and MEP PDs for the fast-frequency band (*A*), for the intermediate-frequency band (*B*), for the slow-frequency band (*C*), and for single units (*D*).

Single-trial decoding of target direction

Given the directional tuning of the fast, intermediate, and slow IEPs, we examined whether reliable target prediction could be achieved on a trial-by-trial basis. Although a wide variety of decoding methods were tested, the linear discriminant analysis (LDA) method was the only one selected for further analysis because its performance was close to or better than that of all the other methods and because it does not require the tuning of arbitrary free parameters.

We separately examined for each frequency band and cortical area how well we could predict target direction from the LFPs. Because the objective of this analysis was to determine the trial-by-trial reliability of directional modulation, we attempted to decode the LFPs recorded only from channels that were determined to be directionally tuned in the earlier stages of our analysis. As described more fully in METHODS, for each pairing of frequency band and cortical area, the activity on each channel was reduced to a set of vectors, where each vector represented the time-varying LFP activity for that pairing on that trial. A single trial could be represented by LFPs from more than one channel by joining the vectors constructed for each channel into one larger vector. We used vectors created with these techniques to estimate the decoding performance of LFPs recorded from a particular channel or combination of channels by estimating the probability that the target direction could be correctly predicted from the LFPs recorded from those channels on a single trial.

For each frequency band, we sought to estimate how the decoding performance varied from channel to channel and for different combinations of more than one channel. We thus tried to decode target direction from multiple random subsets of channels of varying sizes. Because only channels that were directionally tuned were used for this analysis, different numbers of channels were available for the decoding analysis performed on each data set. We used the number of channels that were directionally tuned for a pairing of frequency band and cortical area to determine how many random subsets of channels of each size would be used in that pairing's decoding analysis. For example, for one data set, nine channels in MI were directionally tuned in the slow-frequency band. For that data set we therefore estimated the decoding performance separately for each of nine channels and then estimated the performance for nine randomly selected pairs of channels, and so on, with the final estimate being the decoding performance of all nine channels combined. (The only exception to this procedure came for those data sets for which the number of channels was so large that LDA could not be simultaneously performed on all the channels. In

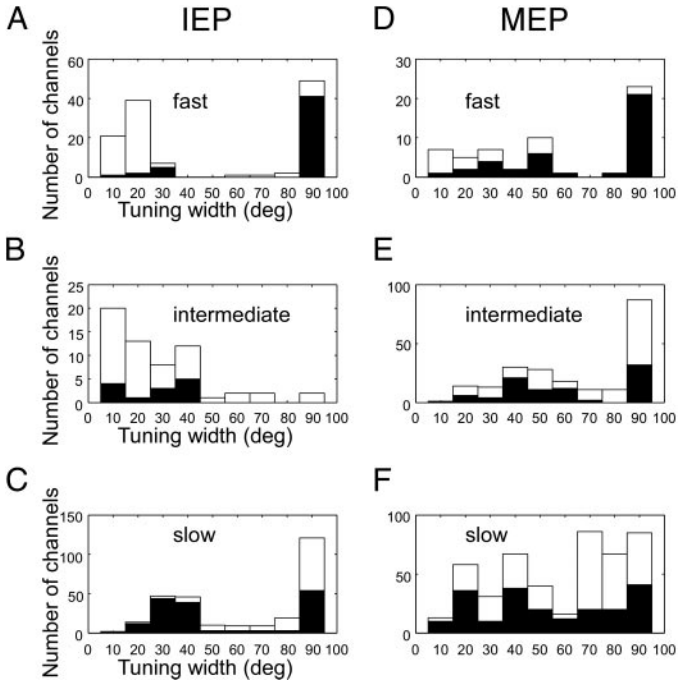

FIG. 10. Distributions of tuning widths of IEPs (*A–C*) and MEPs (*D–F*) for all 3 frequency bands in MI (black bars) and PMd (white bars). Tuning width values represent the best-fit parameter, κ, in the von Mises function for all channels that were well fit to that function ($R^2 > 0.7$).

these cases subsets of the maximum size possible were used.) This method is akin to the "neuron dropping" technique that has been used by other researchers to determine how the performance of the reconstruction of arm movements is affected by the size of the population used for the reconstruction (Wessberg et al. 2000).

As we increased the number of channels used for decoding, the average performance of the classifier would occasionally increase to a maximum and then begin to decrease. This decrease was likely attributable to overfitting because the number of trials in the data sets was not much greater than the number of variables being used for classification in these cases. Therefore we reported the maximum average classification performance versus the number of channels at which the maximum occurred over all data sets in which we observed significant direction tuning (Fig. 11, *A–C*, *left* and *middle*). Maximum classification performance in the fast-frequency band ranged from 9.4 to 18% in MI and from 15.2 to 20.6% in PMd. Because this was an eight-class, classification problem, chance performance was 12.5%. Similarly weak performance was observed in the intermediate-frequency band ranging from 13.7 to 18.7% in MI and from 11.9 to 23.8% in PMd. In contrast, maximum classification performance in the slow-frequency band was typically much stronger, ranging from 18.9 to 41.8% in MI and from 19.2 to 51.3% in PMd, and generally increased with channel count. Interestingly, when examining classification performance versus channel count within a particular data set, performance remained relatively flat in the fast- and intermediate-frequency bands but often increased in the slow-frequency band (Fig. 11, *A–C*, *right*, black lines). We also found that performance within PMd was generally superior to that in MI.

An important issue that has often been neglected in the context of decoding using LFPs is the fact that these signals are highly correlated as a result of so-called noise correlations. Because correlated noise can limit the improvements in decoding performance that can result from the pooling of neural signals (Zohary et al. 1994), using a small number of simultaneously recorded LFPs to predict the decoding performance that can be obtained with a larger number of simultaneously recorded LFPs is potentially problematic (see Lebedev et al. 2005, however, for evidence that correlated activity between neurons is associated with stronger directional tuning). To test whether this problem was relevant to our analysis, we simulated the decoding performance from independently recorded LFP signals by randomly shuffling the trial assignments of the LFP signals across multiple channels/electrodes. Thus for example, data from electrode 1 on trial *i* was associated with data from electrode 2 on trial *j* and so forth for all electrodes, where trials *i* and *j* were recorded during the delay period before movements in the same direction. The performance of the decoding algorithm improved when we artificially removed the noise correlations through the shuffling procedure (Fig. 11, *A–C*, *right*, red lines). In an actual neural prosthesis application, these noise correlations would exist and would thus likely place an upper limit on the decoding performance that could be obtained with LFP recordings.

We also examined the distribution of errors that the decoder made. Confusion matrices were generated that plot the relationship between the actual and decoded directions. Based on the decoding results from one data set, it is weakly evident in the fast- (Fig. 12*A*) and intermediate-frequency (Fig. 12*B*) bands that when an error was made, it was more often made to a neighboring direction than to a more distant direction. This is strongly evident in the slow-frequency band such that there are higher percentages (i.e., brighter elements) in the matrix elements adjacent to the main diagonal (Fig. 12*C*).

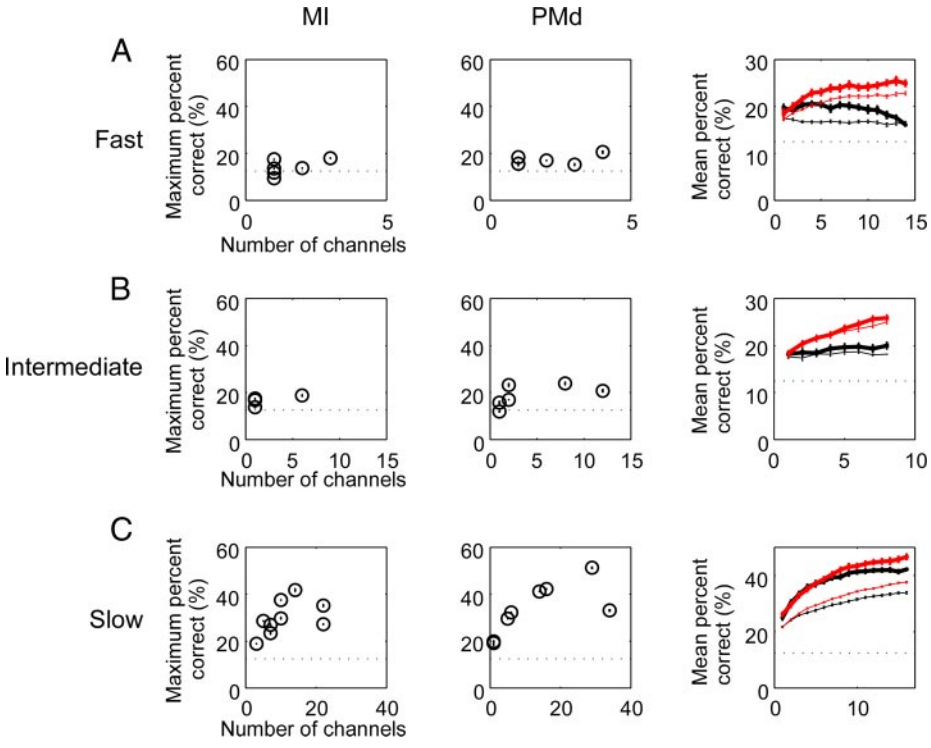

FIG. 11. Performance of the single-trial decoder using the fast, intermediate, and slow oscillations. *A*: maximum average percentage correct classification in the fast-frequency band vs. the number of channels at which the maximum occurred over all data sets (points) in which significant directional tuning occurred in MI (*left*) and PMd (*middle*). Classification performance vs. channel count for one data set (*right*) using MI channels (thin black lines) and PMd channels (thick black lines). Classification performance vs. channel count without "noise" correlations between channels is shown as red lines. Classification performance represents the mean over random combinations of channels. Error bars represent the SE. Chance is at 12.5% (dotted lines). *B* and *C*: same as *A*, but in the intermediate- and slow-frequency bands.

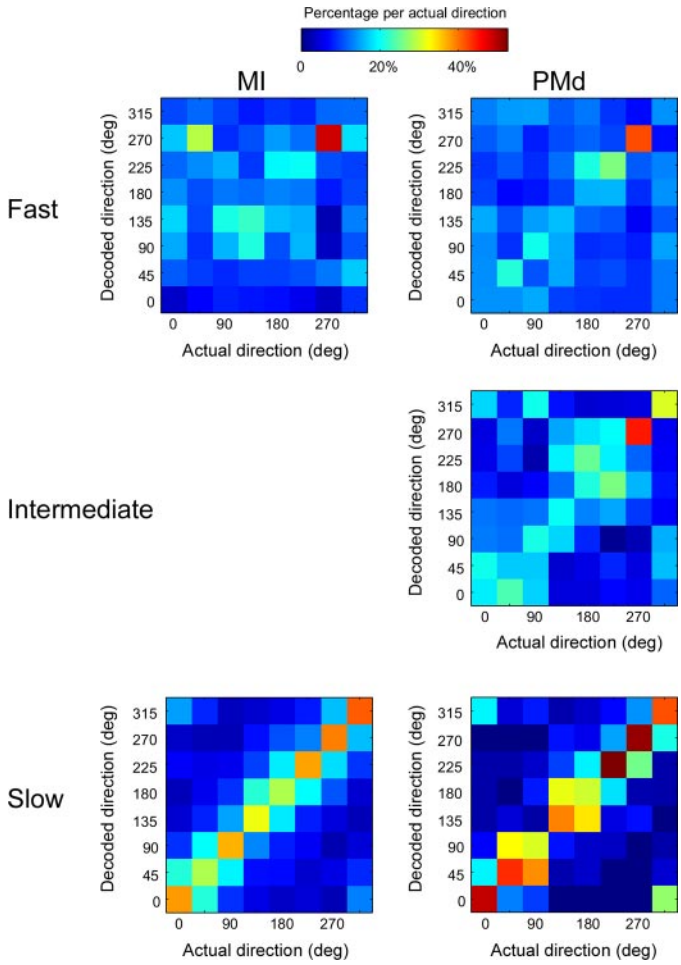

FIG. 12. Confusion matrices for the single-trial decoder based on LFP data from each cortical area and frequency band using results from one data set. In each confusion matrix, each column plots the percentage of trials belonging to a particular direction condition (color coded) that was classified as belonging to each direction condition. For example, the *leftmost column* represents the percentage of actual 0° trials that were decoded as 0, 45, 90, . . . trials. Confusion matrix for the intermediate-frequency band in MI is missing because there were no channels that were directionally tuned for this data set.

DISCUSSION

We have characterized three forms of LFP activity in primary motor and dorsal premotor cortices, phase-locked to the onset of a visually presented signal instructing a reaching movement in a particular direction. Our directional tuning analysis revealed that the fast, intermediate, and slow phase-locked fluctuations were modulated by the direction of the instruction signal, although phase-locking and directional tuning were more prevalent in the slow-frequency band. This directional modulation was further corroborated by predicting the target direction using decoding algorithms applied to single trials of multiple LFP signals. We found only weak decoding performance in the fast- and intermediate-frequency bands but stronger performance in the slow-frequency band. Over all three frequency bands, performance was generally superior in PMd compared with that of MI. As others previously showed in movement-evoked potentials in MI (Mehring et al. 2003), we have demonstrated that specific target/movement directional information is available in early instruction-evoked potentials during movement preparation within MI and PMd. Because our experimental paradigm does not disambiguate between target and movement direction, it is not possible to determine whether the directional tuning of the LFP that we observed is a visual response to the target or a movement planning response.

Variability in preferred directions

The high variability of preferred directions and the weak reliability of tuning across data sets even in the same animal of the fast- and intermediate-frequency IEPs argue that they may be affected by nondirectional factors. On the other hand, the directional tuning of the slow-frequency IEP was evident in all data sets and the preferred directions were relatively consistent across data sets in the same animal. The longer synaptic integration window associated with the slow-frequency IEP may correspond to a larger spatial sampling window involving larger numbers of neurons, which could explain its lower variability and higher reliability.

Clustering of preferred directions

The clustering of preferred directions that we observed in all three frequency bands can be explained in part by the nature of the LFP signal. As others have shown, we observe that LFP signals on different electrodes are highly correlated, presumably as a result of the volume conduction of synchronous postsynaptic potentials from neighboring populations of neurons. Therefore it is perhaps not surprising that the preferred directions of the IEPs are not uniformly distributed but rather form clusters. It should also be noted that we did not observe such clustering or directional biases in the distribution of PDs of single units recorded from the same electrodes (see Fig. 8, *D* and *H*), which suggests that the slow-frequency LFP signal is distinct from the activity of single units.

Partitioning of frequency range

We chose the three frequency bands (<10, 10–25, and 25–45 Hz) primarily based on our observation that local peaks and maxima in LFP spectral power fell into these three bands. In addition, our choice allows for direct comparison with previous research demonstrating oscillations in the intermediate-frequency (about 20 Hz) and fast-frequency (25–40 Hz) bands throughout cortex (Donoghue et al. 1998; Eckhorn et al. 1988; Gray et al. 1989; Jensen et al. 2005; Murthy and Fetz 1992, 1996b ; Singer 1993). Despite the fact that we consistently found local spectral peaks in the intermediate-frequency band, it remains unclear why only one of our animals showed a second prominent peak above 30 Hz. A similar phenomenon was observed by other researchers who found that the peak LFP power could be either between 17 and 26 Hz or between 30 and 39 Hz depending on the animal (Sanes and Donoghue 1993; see also Table 1 in Donoghue et al. 1998). One possibility is that the second peak represents a harmonic of the intermediate-frequency peak. In fact, the second peak is very close to twice the frequency of the intermediate-frequency peak. This would argue that the second peak is not a distinct gamma phenomenon but rather a reflection of lower-frequency beta oscillations. On the other hand, over all our animals we observed that the fast- and intermediate-frequency IEPs exhibited a number of distinct properties including different onset

latencies in the two cortical areas, uncorrelated preferred directions, and different tuning widths. This suggests that the beta- and gamma-frequency bands represent different phenomena, and thus that the gamma-frequency band is not simply a harmonic epiphenomenon of the fundamental beta-frequency oscillation.

Relation to previous research

Our results are consistent with those of Jackson and colleagues who observed similar beta, gamma, and slow (about 10 Hz) fluctuations phase-locked to electrical stimulation of the pyramidal tract (Jackson et al. 2002). Their results suggest that pyramidal tract stimulation antidromically activates collaterals of layer 5 neurons that excite local inhibitory circuits within MI, which then phase-reset ongoing oscillations inherent to motor cortex during the holding period of a precision grip. Our results extend their findings by demonstrating that visual instruction signals also appear to phase-lock ongoing oscillations and fluctuations in a similar fashion.

Our results provide additional evidence that specific visuomotor information is provided by motor cortical LFPs. Two recent studies showed that movement direction can be inferred from LFPs recorded in MI (Mehring et al. 2003; Rickert et al. 2005) by focusing on LFP activity immediately before and after the start of movement (MEPs). Mehring and colleagues (2003) argue that LFPs can provide comparable amounts of information about movement direction as multiunit and single-unit activity by comparing the performance of single-trial decoding. Although we did not directly compare decoding using LFPs and single-unit spikes in this study, our previous work demonstrated that single units could be used to attain decoding performance comparable to the results we have presented here (in the slow-frequency band) using the same behavioral task (Hatsopoulos et al. 2004). Rickert and colleagues (2005) demonstrated that movement-evoked LFPs in at least three different frequency bands provide directional information. They partitioned the frequency axis in a different manner than we did, so their results cannot be completely compared with ours. However, they demonstrated that very slow ($<$4 Hz) and band-pass (6–13 Hz) MEP exhibited strong directional tuning, which is consistent with our results that slow ($<$10 Hz) IEPs provided the strongest directional tuning and the best single-trial decoding performance. However, they found that MEPs in the 16- to 42-Hz range, roughly corresponding to our intermediate- and fast-frequency bands, provided no directional information. Although our results indicated weaker directional modulation in the beta- and gamma-frequency bands, we nonetheless did observe directional tuning in these frequency bands for both IEPs and MEPs.

Noninvasive EEG-based brain–machine interfaces have shown remarkable success in cursor control using slow cortical potentials (Kubler et al. 2001) as well as more recently using the mu (12-Hz) and beta (24-Hz) rhythm amplitudes that appear on EEG electrodes distributed across the scalp (Kubler et al. 2005; McFarland and Wolpaw 2005; Wolpaw and McFarland 2004). In addition, electrocorticographic (ECoG) signals from the surface of the brain of intractable epileptic patients have shown one-dimensional control using mu, beta, and gamma oscillations and off-line two-dimensional prediction of joy-stick position using high gamma oscillations ($>$40 Hz) (Leuthardt et al. 2004). However, it was found that low-frequency ECoG mu rhythms were most effective in predicting movement direction before movement. These ECoG results are consistent with our results in that they indicate that prediction of target direction during movement preparation may be best accomplished using slower-frequency fluctuations, as we have shown, whereas ongoing cursor control may be better achieved using faster oscillations, even $>$40 Hz.

Fast oscillations in the gamma range in the parietal cortex were previously shown to modulate with saccadic eye movement direction in a memory-saccade task (Pesaran et al. 2002). During the memory period, the power of LFP signals between 25 and 90 Hz was tuned to the direction of the upcoming saccadic eye movement. That study also demonstrated that single trials could be decoded using LFP power as accurately as single-unit spikes. However, although not noted in the text of their paper, they did observe low-frequency directional tuning in the LFP during the presentation of the instruction signal as well as several hundred milliseconds later (see Fig. 2 in Pesaran et al. 2002).

At the single-unit level, a minority of neurons in PMd were shown to oscillate in the beta range during the preparation to move (Lebedev and Wise 2000). Moreover, many of these neurons oscillated for only one of two possible upcoming movement directions; that is, the oscillations were directionally selective. Our results using LFPs are consistent with and extend the findings of Lebedev and Wise (2000) in that we show that LFP fast oscillations vary their amplitude in a graded fashion depending on which of eight targets the animal will reach.

Potential role of phase-locked fluctuations

Although the role that these phase-locked fluctuations in motor planning remains unclear, we argue that if oscillations and fluctuations at the LFP level are concurrent with oscillatory (or transient) synchronization of local spiking of single units as other have suggested (Baker et al. 1999; Donoghue et al. 1998; Murthy and Fetz 1996a), these synchronized motor cortical neurons may enhance their influence on postsynaptic targets either in the periphery or in cortex. Experimental evidence has demonstrated that synaptic inputs that arrive synchronously on a postsynaptic neuron are amplified nonlinearly as compared with nonsynchronous inputs (Alonso et al. 1996; Margulis and Tang 1998). Baker et al. (1999) suggested that pyramidal tract neurons that are phase-locked to the beta oscillations may boost their effect on postsynaptic neurons in the spinal cord.

Given the existence of direct and reciprocal projections between PMd and MI, Lebedev and Wise (2000) speculated that synchronized oscillations of PMd neurons might amplify their influence on MI neurons during the preparatory period. Our observation that the fast and slow phase-locked fluctuations in the LFP occur 10–13 ms earlier on average in MI than those in PMd may further support this idea. LFP signals are presumed to represent summed postsynaptic potentials within a local area. If preparatory single-unit activity occurs earlier in PMd (Wise 1985) and fast and slow phase-locked LFP fluctuations within MI in part represent postsynaptic inputs from PMd, one would paradoxically expect to see early phase-locked fluctuations within MI. The later occurrence of these LFP fluctuations in PMd may reflect reciprocal effects from

MI. The fast and slow IEPs also share two directional tuning properties that argue that they may in part have a common source. First, they exhibit directional tuning that is correlated with their MEPs (see Fig. 9), which suggests that these signals may represent direction in a motor coordinate system. Second, their directional tuning widths exhibit a similar bimodal distribution unlike the unimodal distribution observed in the intermediate-frequency band (see Fig. 10).

On the other hand, the intermediate-frequency IEPs occur 8 ms earlier on average in PMd than those in MI. Moreover, we observed no correlation between the directional tuning of the intermediate-frequency IEPs with the corresponding MEPs. We thus speculate that the beta-evoked potentials may represent inputs to the PMd from some source outside the motor cortex (e.g., parietal cortex) representing the target direction or location in a visual coordinate system that then is reflected in MI as a result of direct connections from PMd. Further anatomical and physiological work will be necessary to identify the sources of these signals and to definitively specify the functional role, if any, of their directional modulation.

ACKNOWLEDGMENTS

We thank Z. Haga, J. Joshi, and D. Paulsen for help with the surgical implantation of the arrays, training of monkeys, and data collection; D. Rubino for assistance in the analysis; and M. Fellows and E. Gunderson for help with the surgical procedures.

Present address of J. G. O'Leary: University of California, San Francisco, 513 Parnassus Ave., HSE-802A, Box 0444, San Francisco, CA 94143–0444.

GRANTS

This work was supported by grants from the Whitehall Foundation and the Brain Research Foundation and National Institute of Neurological Disorders and Stroke Grants N01-NS-2-2345 and R01 NS-45853-01A2.

DISCLOSURE

N. G. Hatsopoulos has stock ownership in a company, Cyberkinetics Neurotechnology Systems, Inc., that fabricates and sells the multielectrode arrays and acquisition system used in this study.

REFERENCES

Alonso JM, Usrey WM, and Reid RC. Precisely correlated firing in cells of the lateral geniculate nucleus. *Nature* 383: 815–819, 1996.

Amirikian B, Georgopoulos AP, and Georgopulos AP. Directional tuning profiles of motor cortical cells. *Neurosci Res* 36: 73–79, 2000.

Baker SN, Kilner JM, Pinches EM, and Lemon R. The role of synchrony and oscillations in the motor output. *Exp Brain Res* 128: 109–117, 1999.

Batschelet E. *Circular Statistics in Biology.* New York: Academic Press, 1981.

Crammond DJ and Kalaska JF. Prior information in motor and premotor cortex: activity during the delay period and effect on pre-movement activity. *J Neurophysiol* 84: 986–1005, 2000.

Donoghue JP, Sanes JN, Hatsopoulos NG, and Gaal G. Neural discharge and local field potential oscillations in primate motor cortex during voluntary movements. *J Neurophysiol* 77: 159–173, 1998.

Eckhorn R, Bauer R, Jordan W, Brosch M, Kruse W, Munk M, and Reitboeck HJ. Coherent oscillations: a mechanism of feature linking in the visual cortex. *Biol Cybern* 60: 121–130, 1988.

Fetz EE, Chen D, Murthy VN, and Matsumura M. Synaptic interactions mediating synchrony and oscillations in primate sensorimotor cortex. *J Physiol* (*Paris*) 94: 323–331, 2000.

Fisher N. *Statistical Analysis of Circular Data.* New York: Cambridge Univ. Press, 1993.

Fries P, Reynolds JH, Rorie AE, and Desimone R. Modulation of oscillatory neuronal synchronization by selective visual attention. *Science* 291: 1560–1563, 2001.

Georgopoulos AP, Crutcher MD, and Schwartz AB. Cognitive spatial motor processes 3. Motor cortical prediction of movement direction during an instructed delay period. *Exp Brain Res* 75: 183–194, 1989.

Georgopoulos AP, Kalaska JF, Caminiti R, and Massey JT. On the relations between the direction of two-dimensional arm movements and cell discharge in primate motor cortex. *J Neurosci* 2: 1527–1537, 1982.

Gilbertson T, Lalo E, Doyle L, Di Lazzaro V, Cioni B, and Brown P. Existing motor state is favored at the expense of new movement during 13–35 Hz oscillatory synchrony in the human corticospinal system. *J Neurosci* 25: 7771–7779, 2005.

Gray CM, Konig P, Engel AK, and Singer W. Oscillatory responses in cat visual cortex exhibit inter-columnar synchronization which reflects global stimulus properties. *Nature* 338: 334–337, 1989.

Hatsopoulos N, Joshi J, and O'Leary JG. Decoding continuous and discrete motor behaviors using motor and premotor cortical ensembles. *J Neurophysiol* 92: 1165–1174, 2004.

Jackson A, Spinks RL, Freeman TC, Wolpert DM, and Lemon RN. Rhythm generation in monkey motor cortex explored using pyramidal tract stimulation. *J Physiol* 541: 685–699, 2002.

Jensen O, Goel P, Kopell N, Pohja M, Hari R, and Ermentrout B. On the human sensorimotor-cortex beta rhythm: sources and modeling. *Neuroimage* 26: 347–355, 2005.

Klecka WR. *Discriminant Analysis.* Beverly Hills, CA: Saga Publications, 1980.

Kubler A, Neumann N, Kaiser J, Kotchoubey B, Hinterberger T, and Birbaumer NP. Brain-computer communication: self-regulation of slow cortical potentials for verbal communication. *Arch Phys Med Rehabil* 82: 1533–1539, 2001.

Kubler A, Nijboer F, Mellinger J, Vaughan TM, Pawelzik H, Schalk G, McFarland DJ, Birbaumer N, and Wolpaw JR. Patients with ALS can use sensorimotor rhythms to operate a brain-computer interface. *Neurology* 64: 1775–1777, 2005.

Lebedev MA, Carmena JM, O'Doherty JE, Zacksenhouse M, Henriquez CS, Principe JC, and Nicolelis MA. Cortical ensemble adaptation to represent velocity of an artificial actuator controlled by a brain-machine interface. *J Neurosci* 25: 4681–4693, 2005.

Lebedev MA and Nelson RJ. Rhythmically firing (20–50 Hz) neurons in monkey primary somatosensory cortex: activity patterns during initiation of vibratory-cued hand movements. *J Comput Neurosci* 2: 313–334, 1995.

Lebedev MA and Wise SP. Oscillations in the premotor cortex: single-unit activity from awake, behaving monkeys. *Exp Brain Res* 130: 195–215, 2000.

Leuthardt EC, Schalk G, Wolpaw JR, Ojemann JG, and Moran DW. A brain-computer interface using electrocorticographic signals in humans. *J Neural Eng* 1: 63–71, 2004.

Margulis M and Tang CM. Temporal integration can readily switch between sublinear and supralinear summation. *J Neurophysiol* 79: 2809–2813, 1998.

Maynard EM, Hatsopoulos NG, Ojakangas CL, Acuna BD, Sanes JN, Normann RA, and Donoghue JP. Neuronal interactions improve cortical population coding of movement direction. *J Neurosci* 19: 8083–8093, 1999.

McFarland DJ and Wolpaw JR. Sensorimotor rhythm-based brain-computer interface (BCI): feature selection by regression improves performance. *IEEE Trans Neural Syst Rehabil Eng* 13: 372–379, 2005.

Mehring C, Rickert J, Vaadia E, Cardosa de Oliveira S, Aertsen A, and Rotter S. Inference of hand movements from local field potentials in monkey motor cortex. *Nat Neurosci* 6: 1253–1254, 2003.

Murthy VN and Fetz EE. Coherent 25- to 35-Hz oscillations in the sensorimotor cortex of awake behaving monkeys. *Proc Natl Acad Sci USA* 89: 5670–5674, 1992.

Murthy VN and Fetz EE. Oscillatory activity in sensorimotor cortex of awake monkeys: synchronization of local field potentials and relation to behavior. *J Neurophysiol* 76: 3949–3967, 1996a.

Murthy VN and Fetz EE. Synchronization of neurons during local field potential oscillations in sensorimotor cortex of awake monkeys. *J Neurophysiol* 76: 3968–3982, 1996b.

Pesaran B, Pezaris JS, Sahani M, Mitra PP, and Andersen RA. Temporal structure in neuronal activity during working memory in macaque parietal cortex. *Nat Neurosci* 5: 805–811, 2002.

Pfurtscheller G, Brunner C, Schlogl A, and Lopes da Silva FH. Mu rhythm (de)synchronization and EEG single-trial classification of different motor imagery tasks. *Neuroimage* 31: 153–159, 2006.

Pfurtscheller G, Graimann B, Huggins JE, Levine SP, and Schuh LA. Spatiotemporal patterns of beta desynchronization and gamma synchronization in corticographic data during self-paced movement. *Clin Neurophysiol* 114: 1226–1236, 2003.

Rickert J, Oliveira SC, Vaadia E, Aertsen A, Rotter S, and Mehring C. Encoding of movement direction in different frequency ranges of motor cortical local field potentials. *J Neurosci* 25: 8815–8824, 2005.

Sanes JN and Donoghue JP. Oscillations in local field potentials of the primate motor cortex during voluntary movement. *Proc Natl Acad Sci USA* 90: 4470–4474, 1993.

Scherberger H, Jarvis MR, and Andersen RA. Cortical local field potential encodes movement intentions in the posterior parietal cortex. *Neuron* 46: 347–354, 2005.

Scott SH. Apparatus for measuring and perturbing shoulder and elbow joint positions and torques during reaching. *J Neurosci Methods* 89: 119–127, 1999.

Shah AS, Bressler SL, Knuth KH, Ding M, Mehta AD, Ulbert I, and Schroeder CE. Neural dynamics and the fundamental mechanisms of event-related brain potentials. *Cereb Cortex* 14: 476–483, 2004.

Singer W. Synchronization of cortical activity and its putative role in information processing and learning. *Annu Rev Physiol* 55: 349–374, 1993.

Tallon-Baudry C, Bertrand O, Delpuech C, and Pernier J. Stimulus specificity of phase-locked and non-phase-locked 40 Hz visual responses in human. *J Neurosci* 16: 4240–4249, 1996.

Weinrich M and Wise SP. The premotor cortex of the monkey. *J Neurosci* 2: 1329–1345, 1982.

Wessberg J, Stambaugh CR, Kralik JD, Beck PD, Laubach M, Chapin JK, Kim J, Biggs SJ, Srinivasan MA, and Nicolelis MA. Real-time prediction of hand trajectory by ensembles of cortical neurons in primates. *Nature* 408: 361–365, 2000.

Wise SP. The primate premotor cortex: past, present, and preparatory. *Annu Rev Neurosci* 8: 1–19, 1985.

Wolpaw JR and McFarland DJ. Control of a two-dimensional movement signal by a noninvasive brain-computer interface in humans. *Proc Natl Acad Sci USA* 101: 17849–17854, 2004.

Zohary E, Shadlen MN, and Newsome WT. Correlated neuronal discharge rate and its implications for psychophysical performance. *Nature* 370: 140–143, 1994.